PERGAMON

Aerosol Science 34 (2003) 1277–1296

Journal of
Aerosol Science

www.elsevier.com/locate/jaerosci

The AIDA soot aerosol characterisation campaign 1999

H. Saathoff[a,*], O. Moehler[a], U. Schurath[a], S. Kamm[a], B. Dippel[b], D. Mihelcic[c]

[a] *Institut für Meteorologie und Klimaforschung, Forschungszentrum Karlsruhe, P.O.B 3640, Karlsruhe D-76021, Germany*

[b] *Institut für Troposphärenforschung, Permoserstr. 15, Leipzig D-04318, Germany*

[c] *Institut für Chemie und Dynamik der Geosphäre, Forschungszentrum Jülich, P.O.B 1913, Jülich D-52425, Germany*

Received 27 June 2002; accepted 29 January 2003

Abstract

An intensive soot aerosol characterisation campaign was organised in October 1999 at the large aerosol chamber facility AIDA in Karlsruhe, with the participation of scientists from nine Austrian, German, Russian, and Swiss Research Centres and Universities who contributed special equipment and expertise. The main goal was a comprehensive physical and chemical characterisation of soot aerosol from a modern turbo Diesel passenger car equipped with an oxidation catalyst, in comparison with artificial soot aerosol ("Palas" soot) from a commercial spark discharge generator which is often used as a surrogate for combustion soot in laboratory studies. Included were experiments with pure ammonium sulphate aerosol as well as its external mixtures with soot aerosols, and their evolution to partially internal mixtures on time scales up to 45 h. Effects of organic coatings on various aerosol properties, generated in situ by heterogeneous nucleation of products from the reaction of α-pinene with ozone were also investigated. The purpose of this paper is to present an overview of the whole campaign. This includes the description of technical and modelling tools, standard procedures, and the presentation of experimental parameters in tabular form, as a common background for a series of companion papers which focus on selected scientific issues. Included is a comparison between Diesel and spark generated soot in terms of their Raman and ESR spectra. The most remarkable difference is the large spin density in spark generated soot, which exceeds that of Diesel soot by an order of magnitude. However, the spin densities in both materials are too small to affect the surface properties of soot aerosols to a significant extent.

Keywords: Diesel soot; Spark generated "Palas" soot; ESR; Raman

* Corresponding author. Tel.: +49-7247-82-2897; fax: +49-7247-82-4332.
E-mail address: harald.saathoff@imk.fzk.de (H. Saathoff).

0021-8502/$ - see front matter © 2003 Elsevier Ltd. All rights reserved.
doi:10.1016/S0021-8502(03)00363-X

1. Introduction

Most inorganic (e.g. sulphates, nitrates) and organic aerosols (e.g. diacids) do not absorb solar radiation, thus giving rise to negative radiative forcing by scattering incoming solar radiation back into space (IPCC, 2001). In sharp contrast, soot aerosols are poor scatterers but extremely efficient absorbers of solar radiation due to their black carbon (BC) content, thus giving rise to positive forcing. This effect has recently been discovered to be important over the Indian ocean during the winter monsoon season when large amounts of anthropogenic aerosols containing more than 10% BC are advected from the Indian subcontinent (Lelieveld et al., 2001; Rajeev & Ramanathan, 2001). The combination of sea surface cooling with radiative heating of the boundary layer through absorption of solar radiation by soot may substantially perturb the regional hydrological cycle. It is thus important to characterise the optical properties of soot and their possible modifications due to physical (e.g. compaction, transition from external to internal mixing with non-absorbing particles) and chemical processes (e.g. surface oxidation, coating), as well as the impact of such modifications on their hygroscopic properties.

Globally large amounts of soot aerosols are emitted into the troposphere as a result of fossil fuel combustion (Cooke, Liousse, Cachier, & Feichter, 1999) and biomass burning (Kuhlbusch et al., 1996). The source strength of the associated mass fraction of BC is estimated to be in the order of 12–14 Tg C yr^{-1} (Liousse et al., 1996; Cooke & Wilson, 1996), with a large uncertainty range (Cooke et al., 1999). The atmospheric residence time of BC is estimated to range between < 4.5 and 10 days (Cooke & Wilson, 1996; Koch, 2001), depending on the conversion rate of the hydrophobic particles into more hydrophilic ones which can be removed from the atmosphere by incorporation into cloud droplets and wet deposition. Very low BC concentrations, typically in the order 0.5 ng m^{-3}, are found in the lower stratosphere (Blake & Kato, 1995; Pueschel et al., 1997; Strawa et al., 1999) and in polar regions. Several 100 ng m^{-3} BC have been reported for continental background air (Pakkanen et al., 2000), while BC concentrations in the order of 1 μg m^{-3} are typical of rural source areas (Liousse et al., 1996). Highest BC concentrations, occasionally approaching or even exceeding 20 μg m^{-3}, occur in polluted urban air (Dod et al., 1986; Hansen & Novakov, 1990; Heintzenberg & Winkler, 1991; Berghmans, Pauwels, Roekens, & Bogaert, 1996; Hitzenberger & Tohno, 2001; Streets et al., 2001).

The mass fraction of black or elemental carbon in the sub-micron particle size range amounts to a few percent (Heintzenberg & Winkler, 1991), but may exceed 10%, depending on the source region (Lelieveld et al., 2001; Hitzenberger & Tohno, 2001). In Europe and the US, soot aerosol emissions are dominated by Diesel trucks and Diesel passenger cars which contribute up to 10 μg m^{-3} BC to the aerosol load in polluted urban areas (Israel, Schlums, Treffeisen, & Pesch, 1996). While modern Diesel engines emit much less soot aerosol mass than older designs, emissions of nanoparticles seem to have simultaneously increased in terms of number concentrations (Kittelson, 1998). Adverse health effects correlate more strongly with the mass of particles less than 10 μm in diameter (PM10) than with any other type of pollutant. This provides a strong motivation to investigate specific properties of soot particles which are nearly exclusively found in the fine particle range (Hitzenberger & Tohno, 2001). The correlation with adverse health effects becomes even more pronounced for particles below 2.5 μm, PM2.5 (Dockery et al., 1993; Pope III et al., 1995; Schwartz, 1993; Peters, Wichmann, Tuch, Helnrich, & Heyder, 1997; Wichmann & Peters, 2000; Kaiser, 2000; Morawska, 2001),

implying that soot particles with their exceedingly large specific surface area may be the culprit. See, however, Stöber and Abel (1996).

It has also been speculated that the large specific surface area of fresh fractal soot particles could promote heterogeneous chemical reactions of atmospheric trace gases and radicals (Ravishankara & Longfellow, 1999; Jacob, 2000; Grassian, 2001). While recent laboratory experiments indicate that most of the proposed reactions are less effective than previously assumed (Kamm, Möhler, Naumann, Saathoff, & Schurath, 1999; Disselkamp, Carpenter, & Cowin, 2000a, b; Kirchner, Scheer, & Vogt, 2000; Saathoff et al., 2001), it is still important to understand the process of particle surface aging due to heterogeneous chemical reactions, as they may change the optical and/or hygroscopic properties of soot.

The physical and chemical properties of various soot aerosols have been investigated in a number of laboratories, often with inconsistent results. A major source of uncertainty relates to the use of different types of soot in different laboratories. The intercomparability could be improved if a highly reproducible "reference" soot aerosol generator was available. Many researchers have chosen a commercially available spark discharge generator (GfG 1000, Palas) for this purpose (Helsper et al., 1993). However, a comprehensive intercomparison study of "Palas" reference soot with soot aerosol exhausted by a modern Diesel passenger car engine under realistic operating conditions is not yet available. This motivated us to use the large aerosol chamber AIDA of Forschungszentrum Karlsruhe for such an intercomparison study.

This paper is organised as follows: After a technical description of the aerosol chamber and methodologies of aerosol preparation for the campaign, the available physico-chemical, optical, chemical, and modelling tools for their comprehensive characterisation are briefly presented. Special emphasis is given to an intercomparison study between "Palas" and Diesel soot on the basis of their Raman and ESR spectra, including spin density measurements. This section is followed by a short guided tour through the organisation of the campaign: 10 experiments were arranged in three groups, each focussing on a scientific goal of the campaign. Since a comprehensive discussion of the results would be beyond the scope of an introductory paper, the reader is referred to a series of specific companion papers which cover different issues of the campaign.

2. Experimental

2.1. Description of the AIDA facility

A schematic drawing of the AIDA facility (AIDA means: Aerosols, Interactions and Dynamics in the Atmosphere) which is situated in a large circular building of 17 m diameter and 13 m height (Bunz et al., 1996; Kamm et al., 1999) is shown in Fig. 1. The aerosol reactor is a cylindrical aluminium vessel of 84.3 m^3 volume and 4 m inner diameter. It is mounted in an upright position in a thermally isolating chamber. The air inside the chamber walls which are made of 200 mm polyurethane foam can be forced through heat exchangers and circulated through two vertical ventilation shafts to stabilise the reactor at any desired temperature in the range $+60°C$ to $-90°C$. The facility is surrounded by three working platforms L1–L3 which render access to reactor flanges of various sizes. The flanges are used for gas/aerosol injection and sampling, or for in situ optical analysis. For example, the cross-sectional view in the lower part of Fig. 1 shows two fourier transform (FT) spectrometers (IFS66, Bruker) on working platform L2. White mirror systems are mounted

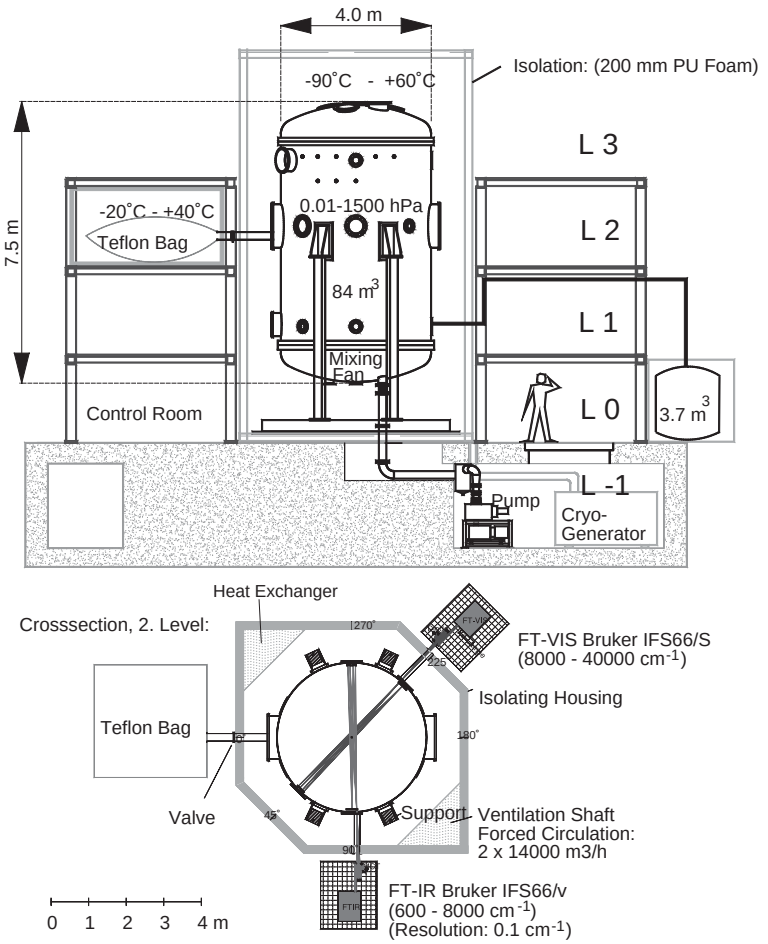

Fig. 1. Schematic of the AIDA facility.

inside the chamber on opposite flanges, increasing the optical path to a maximum of 254 m. The FT spectrometers cover the infrared and ultraviolet-visible spectral ranges. The participating scientists, their affiliations, and their scientific contributions are listed in Table 1. The arrangement of instruments, sampling devices, and other equipment on the working platforms is given in Table 2. Gases and aerosols were sampled through stainless steel tubes which ranged 40 cm into the reactor.

The soot intercomparison campaign totalled to 10 experiments (Table 3) which were carried out on time scales of 13–45 h at ambient pressure, temperatures of 297 ± 1 K, and initial relative humidities around 45%. Prior to the campaign the aluminium walls of the aerosol reactor had been preconditioned by exposing them to 100 ppm ozone in air over night. Before each individual experiment the reactor was evacuated to 0.02 hPa, flushed twice with 10 hPa synthetic air, and filled to ambient pressure with humidified particle free synthetic air (low hydrocarbon grade, Linde). Aerosol was added when the air temperature had equilibrated with the chamber walls. A mixing fan of 50 cm diameter, located near the bottom of the chamber, provided homogeneous mixing within 5 min when operated at 360 rpm. During the initial and final 2–3 h of each experiment the aerosol

Table 1
Participating groups and their major contributions

Participants	Leading institutions	Specific contributions
Ernest Weingartner, Niklaus Streit, Urs Baltensperger	Laboratory for Atmospheric Chemistry, Paul Scherrer Institute (PSI), Switzerland	Measurements of hygroscopic growth, "Fuchs" surface area, total aerosol mass, BC contents (aethalometry, photoelectric charging), EC contents by thermal analysis
Ulf Kirchner, Volker Scheer, Rainer Vogt	Ford Research Center Aachen, Germany	Surface sensitive analysis of single particles using laser desorption/ionisation mass spectrometry
Bernd Dippel	Institute for Tropospheric Research (IfT), Leipzig, Germany	Nd-YAG laser-induced Raman spectroscopy of soot
Hauke Gorzawski, Stefan Weinbruch	Institute for Mineralogy, Technical University of Darmstadt, Germany	Comprehensive studies of particle micro-and nanostructures by TEM/HRTEM
Helmuth Horvath	Institute for Experimental Physics, University of Vienna, Austria	Optical absorption measurements of soot by integrating plate method
Lutz Krämer, Zoltan Bozoki, Ulrich Pöschl	Institute of Hydrochemistry, Technical University of Munich, Germany	BC measurements using photoacoustic detection
Harald Saathoff, Martin Schnaiter, Werner Schöck, Karl-Heinz Naumann, Ulrich Schurath, Ottmar Möhler Stefan Kamm	Institute for Meteorology and Climate Research, Forschungszentrum Karlsruhe, Germany	Aerosol chamber operation, generation, conditioning, organic coating and characterisation of aerosols: number concentration, size distribution, chemical composition, TC. Measurements of optical properties (uv-vis-ir), modelling of aerosol dynamics and optical properties
Carsten Natzeck, Joachim Goschnik	Institute for Instrumental Analytics, Forschungszentrum Karlsruhe, Germany	Surface sensitive/depth resolving analysis of particulate material; generation of Diesel engine soot
Djuro Mihelcic	Institut für Chemie und Dynamik der Geosphäre, Forschungszentrum Jülich	Esr spectroscopy of soot
Olga Popovitcheva	Moscow State University	Water adsorption and energetic properties of "Palas" soot

was comprehensively characterised by as many techniques as were available. While the initial and final periods of intensive aerosol sampling gave rise to significant chamber dilution, the aerosol was left almost undisturbed in between these periods. A large Teflon bag served as a buffer volume to maintain the chamber contents at ambient pressure. It communicated with the chamber via a stainless steel tube of 200 mm i.d., as shown in Fig. 1. Dry synthetic air was added occasionally to compensate for sampling losses, which caused the relative humidity to drop accordingly. Water vapour was measured with an optical dew point sensor (1311DR, General Eastern).

Table 2
Instrumentation of the AIDA facility during the soot characterisation campaign

Level	Institute	Instrumentation
L3	IMK	11 stage rotating disc low pressure impactor (LPI-ROT 25/0018, Hauke)
	IMK	Filter sampling system (vacuum filter holders and calibrated mass flow controllers)
	IMK	Condensation particle counter (CPC 3022A, TSI)
	IMK	Optical dew point sensor (1311DR, General Eastern)
L2	IMK	FTIR (IFS 66/v, Bruker) and FTVIS (IFS 66/s, Bruker) both for 'in situ' measurements with White cell optics providing up to 254 m optical path
	IMK	Extinction Tube (230–1000 nm, 5 m optical path) with white light source (DH-2000-FHS, Avantes), fibre optics, and Zeiss spectrometers (MCS 55)
	IMK	Extinction cell (473 nm diode, 75 m optical path, home made)
	IMK	Nephelometer (3563, TSI) working at 450, 550, and 700 nm
	IMK	Extinction (662 nm, 4 m path) for 'in situ' monitoring
	IMK	Teflon bag (ca. 2 m^3), serving as buffer volume
L1	IMK	2 spark discharge soot generators (GfG 1000, Palas)
	IMK	Ultrasonic nebulizer (GA 2400, Sinaptec) & diffusion dryers (home made)
	IFIA	Injection port and 100 m PVC pipeline connecting aerosol chamber with VW Diesel Engine exhaust system via 3 denuders (home made)
	IMK	DMA (3071, TSI) + CPC (3010, TSI) and CPC (3022A, TSI)
	PSI	Hygroscopicity Tandem Differential Mobility Analyser (H-TDMA) + diffusion dryer
	PSI	2 aethalometers (AE10 and AE30, MAGEE Scientific)
	TUM	Photo-Acoustic Soot Sensor (PASS)
	PSI	Betameter (FH-62-I-R, Eberline)
	PSI	Photoelectric Aerosol Sensor (PAS 2000, EcoChem)
	PSI	Diffusion charger (LQ1-DC, Matter Engineering)
	PSI	Combination of DMA (3071, TSI) and optical particle counter (LAS-X, PMS)
	IMK	Gas handling manifold (home made)
	IMK	Ozone generator (Semozon 030.2, Sorbios)
	IMK	Trace gas monitors for O_3 and NO/NO_x (O3-41M, Environment; APNA-300E, Horiba; ML9841, Monitor Labs)
L0	Ford	Laser Mass Analyser for Particles in the Airborne State (LAMPAS)
	IMK	Mixing fan (500 mm diameter)
	IMK	Central data acquisition system (T, P, r.h., monitor data, etc.) based on IMP modules and Propack software (Solatron)
	IMK	Air humidifier (home made) and particle filter (Dillmann, Bier, Linder, & Schubert, 1987)
L-1	IMK	Vacuum pumps (DP180 and EH2600, Edwards)
	IMK	Cooling system (230'/40DU/90LN2, Weiss Umwelttechnik)

IMK: Institute for Meteorology and Climate Research, IFIA: Institute for Instrumental Analytics, PSI: Paul Scherrer Institute, TUM: Technical University Munich, Ford: Ford Research Centre Aachen.

2.2. Preparation of aerosols and gas handling

Two spark discharge generators (GfG, Palas) were operated at their maximum frequency settings to supply the AIDA chamber with 100 $\mu g\,m^{-3}$ soot aerosol ("Palas" soot) in about 90 min. Argon

Table 3
Experiments carried out during the AIDA soot campaign in October 1999. The temperature was (297 ± 1) K in all experiments. CMD = initial count mean diameter

Date	No.	I. Comparison of Diesel and "Palas" soot aerosols
4–5 October	1	Palas soot, ca. 100 μg/m^3 in dry synthetic air, CMD 241 nm, duration of experiment: 26 h.
6–8 October	2	Diesel soot, ca. 70 μg/m^3, CMD 255 nm, NO_x concentration ca. 20 ppb, 43.2–32.7% r.h., duration: 45 h.
11–13 October	3	Palas soot, ca. 100 μg/m^3, CMD 203 nm, NO_x concentration ca. 60 ppb, 46.8–38.0% r.h., duration: 44 h.
		II. Ageing of mixtures of Diesel soot and $(NH_4)_2SO_4$ aerosols
14–15 October	4	Pure $(NH_4)_2SO_4$-aerosol, ca. 760 μg/m^3, initial size distribution cf. Fig. 2, 48.2–43.0% r.h., duration: 26 h.
18–19 October	5	Initially external mixture of Diesel soot with $(NH_4)_2SO_4$ aerosol, ca. 50/140 μg/m^3, 44.9–35.9% r.h., duration: 26 h.
20–22 October	6	Initially external mixture of $(NH_4)_2SO_4$ with Diesel soot aerosol, ca. 1500/100 μg/m^3, 45.7–36.5% r.h., duration: 45 h.
		III. Organic coating of soot and $(NH_4)_2SO_4$ aerosols
25–26 October	7	Diesel soot, ca. 80 μg/m^3, CMD 290 nm, + ca. 470 ppb ozone, + 61 ppb α-pinene, 45.3–36.2% r.h., duration: 18 h.
26–27 October	8	$(NH_4)_2SO_4$-aerosol, ca. 700 μg/m^3, CMD 372 nm, ca. 700 μg/m^3), + ca. 470 ppb ozone + 61 ppb α-pinene, 47.5–38.8% r.h., duration: 14 h.
27–28 October	9	Palas soot, ca. 110 μg/m^3, CMD 261 nm, + ca. 470 ppb ozone, + 61 ppb α-pinene, 45.0–35.0% r.h., duration: 13 h.
28–29 October	10	Organic aerosol, ca. 65 μg/m^3, CMD 60 nm, generated from ca. 470 ppb ozone + 61 ppb α-pinene, 42.9–34.5% r.h., duration: 14 h.

was used as carrier gas (99.9999%, Messer Griesheim) at a flow rate of 5 1/min per generator. The size distribution of the primary carbon particles is known to depend on these operating conditions (Schwyn, Garwin, & Schimdt-Ott, 1988). After passing the output of the generators through a coagulation tube of 0.5 m length and 40 mm i.d., "Palas" soot aerosol was directly injected into the aerosol chamber.

Diesel soot aerosol was generated with a Volkswagen 4 cylinder turbo Diesel engine (TDI, type 1Z) with 1.9 l capacity, 66 kW maximum power, direct fuel injection, and supercharger. The engine was equipped with a complete exhaust system including recycling of exhaust gases, and an oxidation catalyst. To simulate real operating conditions the engine was attached to an eddy current brake. The engine was operated at 2500 rpm with a load of 17 kW. Typical exhaust gas temperatures ranged between 250°C and 270°C. The Diesel fuel contained 383 mg S/kg fuel (DIN EN 24260), and had an aromatics content of 29.5 wt%. Five litre per minute (STP) of the exhaust gas were sampled via a T-fitting at the tailpipe and immediately diluted 1:10 with synthetic air by an isokinetic dilution system (VKL 10, Palas). The diluted aerosol contained 4–8 mg TC m^{-3} and about 2.9 μmol m^{-3} sulphate, and relative humidities ranged from 5% to 20% at temperatures between 30°C and 21°C. Sub-stoichiometric amounts of ammonium ions were also found, probably due to contamination of the filter samples with ammonia gas from the ambient air.

To avoid unrealistically high trace gas concentrations in the AIDA chamber the dilute aerosol was passed through three denuders in series. Each denuder consisted of a hermetically sealed stainless

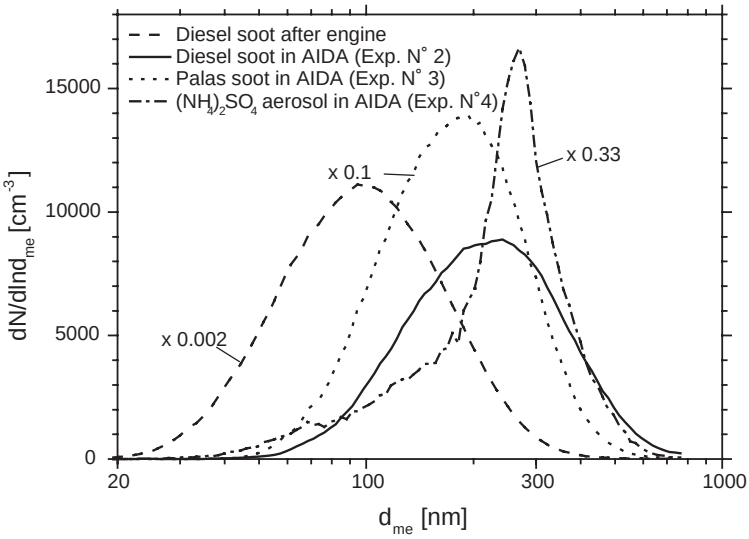

Fig. 2. Typical initial size distributions of Diesel soot (solid line), "Palas" soot (dotted line), $(NH_4)_2SO_4$ (dash dotted line) in the AIDA chamber, and of Diesel soot measured at the engine directly after 1:10 dilution of the exhaust aerosol.

steel box $400 \times 400 \times 2000\ mm^3$ in size, which contained 16 pipes of 1.5 m length and 40 mm i.d. made of stainless steel mesh. The pipes were embedded in ca. 200 l granular adsorbent material. The first denuder was filled with molecular sieve to remove water vapour; volatile organic compounds were removed by adsorption on activated charcoal in the second denuder; the third denuder contained cobalt oxide coated ceramic granulate to remove most of the NO_x (Arens, Gulzwiller, Baltenesperger, Gäggeler, & Ammann, 2001). From filter samples collected up- and downstream of the denuder battery it was found that, on average, 2/3 of the carbon and sulphur aerosol mass was lost. The output of the denuder battery was conducted through 100 m of 45 mm i.d. PVC tubing to the AIDA facility, where between 2 and 3 m^3 of the aerosol were injected into the reaction chamber. This yielded between 50 and 100 $\mu g\ m^3$ carbon aerosol which was contaminated with less than 10 ppb $NO + NO_2$. Infrared spectra of Diesel soot collected on Teflon filters up- and downstream of the denuder battery and in the AIDA chamber, and analysed as described by Kirchner, Vogt, Natzeck, and Goschnick (2003) did not show significant differences in surface functionalities.

Ammonium sulphate aerosol was generated by dispersing dilute aqueous solutions of $(NH_4)_2SO_4$ with an ultrasonic nebulizer (GA 2400, Sinaptec). The output was passed through two diffusion driers in series, which yielded an aerosol of nearly spherical dry ammonium sulphate particles. For example, dispersion of a 1 wt% $(NH_4)_2SO_4$ solution resulted in an aerosol with a mobility equivalent count mean diameter of about 250 nm.

Fig. 2 shows initial size distributions of ammonium sulphate and Diesel soot aerosols in the AIDA chamber, as well as a size distribution at the tailpipe of the engine. The distribution in the AIDA chamber is shifted to larger sizes due to coagulation in the denuder battery and in the transfer line. Initial count mean diameters and mass concentrations of soot and ammonium sulphate aerosols in the AIDA chamber are also listed in Table 3.

Organic particle coatings and/or secondary organic aerosols (SOA) were generated in situ by adding 61 ppb α-pinene vapour (~5 hPa litre) to the chamber which already contained ca. 500 ppb ozone in the presence of a seed aerosol, or in particle-free air. Ozonolysis of α-pinene is known to yield 4.5 mol% pinic acid as the least volatile product (Koch et al., 2000), which either nucleates heterogeneously on the seed aerosol, or forms new particles by homogeneous nucleation. The organic aerosol mass is enhanced by co-condensation of other more volatile oxygenated products, in particular pinonic acid (Koch et al., 2000; Griffin, Cocker III, Flagan, & Seinfeld, 1999; Yu, Cocker III, Griffin, Flagan, & Seinfeld, 1999), see the companion paper by Saathoff et al. (2003b).

The concentrations of α-pinene, ozone, and sulphate aerosol were monitored in situ and quasi-continuously by long path FTIR spectrometry (Bruker IFS 66v, 254 m folded optical path, spectral range 4000–800 cm^{-1}, spectral resolution 0.125 cm^{-1}). The instrument was also used to monitor chamber dilution after adding 30 ppb SF_6 (99.9%, Messer Griesheim) as an inert tracer. Background measurements taken before and after each experiment showed no significant influence of particles deposited on the mirrors of the multi-pass cell. Discontinuous measurements of ozone and NO/NO_x were carried out with commercial monitors (Environment O_3-41M; Horiba APNA-300E; Monitor Labs ML9841).

Chamber wall effects have been investigated earlier (Kamm et al., 1999; Saathoff et al., 2001) and are taken into account by the COSIMA model. The loss of SOA precursor material to the chamber walls can be neglected since the first-order rate coefficient for deposition on the particles is two orders of magnitude larger than for diffusion-limited loss to the walls. The aerosol particle lifetimes in the AIDA chamber, 1–2 days for compact sub-micron particles and between 7 and 12 days for fractal soot particles, are comparable or longer than the experimental timescale of 1–2 days for these experiments.

3. Aerosol diagnostics and modelling tools

During each experimental run the characteristics of aerosols contained in the AIDA chamber as well as their evolution in time were characterised as completely as possible, using the diagnostic tools and experimental techniques listed in Table 2. Because most of the instruments could not be operated continuously to avoid excessive chamber dilution, the physico-chemical aerosol simulation code COSIMA (Naumann & Bunz, 1992) was utilised to model the time evolution of particle number concentrations, size and surface area distributions, and optical particle properties. Details can be found in two companion papers (Naumann, 2003; Wentzel, Gorzawki, Naumann, Saathoff, & Weinbruch, 2003).

3.1. Number densities, size distributions, and chemical composition

Number densities of particles larger than 7 nm were measured continuously with two condensation particle counters (CPC 3022A, TSI) on levels L1 and L3 to make sure that the chamber was homogeneously mixed. During the initial and final intensive sampling periods size distributions were measured on level L1 with a scanning mobility particle sizer (DMA 3071 & CPC 3010, TSI), together with total aerosol mass determinations with a betameter (FH-62-I-R, Eberline). Samples for total carbon/elemental carbon analysis were collected on preheated quartz fibre filters (∅ 47 mm,

MK 360, Munktell/∅25 mm, Schleicher Schüll), and were analysed with coulometric technique (TC) (Coulomat 702, Ströhlein) and a thermal method (Lavanchy, Gäggeler, Nyeki, & Baltensperger, 1999). Teflon filters (47 mm, PTFE, 0.2 μm pore size, Sartorius) were used to collect samples for ion chromatographic analysis. The sampling periods can be looked up in Table 1 of the companion paper by Saathoff et al. (2003a).

3.2. Aerosol optical measurements

In addition to the in situ extinction measurements with the FTIR spectrometer (see Section 2.1) a Helium Neon laser (662 nm) was sent across the AIDA vessel resulting in 4 m pathlength. Aerosol extinction was also determined periodically at 473 nm by means of an external White type optical cell (75 m folded path length, sensitivity $\sim 10^{-5}$ m^{-1}). The cell was run in series with a 5 m long optical flow tube which covered the spectral range 230–1000 nm at 2.5 nm spectral resolution (sensitivity $\sim 10^{-4}$ m^{-1}), and with an integrating nephelometer (3563, TSI) which yielded scattering and backscatter parameters at 450, 550, and 700 nm. Absorption coefficients were determined by analysing filter samples with the integrating plate method (Horvath, 1997). Furthermore mono disperse aerosol particles of 400 nm diameter were selected by a DMA (3071, TSI) and analysed with an optical particle counter (LAS-X, PMS) using scattering of 662 nm laser light (Weingartner et al., 2000). To quantify the absorbing black carbon (BC) a photo acoustic soot sensor (PASS) (Krämer, Bozoki, & Niessner, 2001) and two aethalometers (AE10 and AE30, MAGEE Scientific) were used (Weingartner et al., 2003). A detailed account of the optical measurements and the obtained results is given in the companion papers by Schnaiter et al. (2003) and Weingartner et al. (2003).

3.3. Surface sensitive diagnostics

The full range of surface sensitive techniques available during the AIDA campaign are comprehensively covered in a companion paper (Kirchner et al., 2003), and only a brief account is given here: A LAMPAS-2 system (laser mass analyser for particles in the airborne state) was available to analyse single size-selected aerosol particles with a pulsed nitrogen laser ($\lambda = 337$ nm). The soft ionisation conditions make this mass spectrometer particularly sensitive to surface functionalities and particle coatings (Trimborn, Minz, & Spengler, 2000). Further information on surface functionalities of soot particles collected on PTFE filters (47 mm, 0.2 μm pore size, Sartorius) was obtained by transmission FTIR spectroscopy, after transferring the deposited material onto KBr windows.

Several depth profiling techniques were available to characterise size-segregated aerosol samples which had been collected on indium foils with a Berner cascade impactor. These techniques were SNMS (Secondary Neutral Mass Spectrometry), QMS-SIMS (Secondary Ion Mass Spectrometry with a Quadrupole Mass Spectrometer), TOF-SIMS (Time Of Flight-Secondary Ion Mass Spectrometry), and XPS (X-ray excited Photoelectron Spectroscopy). Details are given in the companion paper by Kirchner et al. (2003).

A Photoelectric Aerosol Sensor (PAS 2000, EcoChem) was used as a specific soot particle detector. The response of the instrument, which is based on photoelectron emission charging of soot particles by 222 nm radiation, is correlated with the amount of surface-adsorbed polycyclic aromatic hydrocarbons (Burtscher, 1992; Burtscher & Siegmann, 1994). In the absence of polycyclic hydrocarbons a weak signal remains due to the significantly lower photoelectric yield of elemental carbon

(Baltensperger, Weingartner, Burtscher, & Keskinen, 2001). The Fuchs surface area of the fractal soot particles was measured simultaneously with a diffusion charger (LQ1-DC, Matter Engineering AG) (Matter, Siegmann, & Burtscher, 1999; Baltensperger et al., 2001). Results are reported by Saathoff et al. (2003b).

Adsorption/desorption isotherms of water on "Palas" soot were measured by Kuznetsov, Rakhmanova, Popovitcheva, and Shonia (2003). Furthermore, they employed thermodesorption of nitrogen to determine the specific surface area of "Palas" soot. For these studies "Palas" soot was collected in mg amounts directly from the spark discharge generators of the AIDA facility.

Also related with the surface properties of soot particles is their hygroscopic behaviour. Growth factors of dried and size-selected soot particles in the range 50–250 nm, which were measured at 90% relative humidity with a Hygroscopicity-Tandem Differential Mobility Analyser (H-TDMA, Weingartner, Gysel, & Baltensperger, 2002; Gysel, Weingartner, & Baltensperger, 2002), are reported in a companion paper (Saathoff et al., 2003b).

3.4. Micro- and nanostructural information

The fractal structure of soot particles and the nearly spherical shape of ammonium sulphate particles, which had been collected on polycarbonate filters (47 mm, Nuclepore, type 111106, Corning), were readily visualised by scanning electron microscopy (SEM, JSM-840, Jeol). However, since this instrument does not resolve the size and shape of the soot primaries, aerosol particles were also collected on nickel TEM grids with conducting formvar foil by means of a three-stage cascade impactor, and analysed with a Transmission Electron Microscope (TEM, CM12, Philips). The internal nanostructure of the soot primaries could be partially resolved with a High Resolution Transmission Electron Microscope (HRTEM, CM20, Philips). Both instruments had EDX capability for elemental analysis (Wentzel et al., 2003).

3.5. Raman and electron spin resonance (ESR) spectroscopy of soot aerosol

It is well known that Raman spectra of soot particles, which are excited in most cases with a visible line of an Ar^+ laser, consist of a broad so-called G-band with a stokes shift of about 1580 cm^{-1} (G for "graphite"), and a still broader D-band around 1360 cm^{-1} (D for "disordered", since it corresponds to a Raman transition which is forbidden in pure graphite) (Sze, Siddique, Sloan, & Escribano, 2001). Following the early work of Tuinstra and Koenig (1970), the band area ratio I_G/I_D has often been used as an indicator of the mean size L_a of the graphitic sub-units (Wakayama et al., 1999) which have also been observed in HRTEM pictures of the turbostratic Diesel soot primaries (cf. Figs. 2 and 3 in the companion paper by Wentzel et al., 2003). More recently, however, the validity of this simple relationship has been questioned (Ferrari & Robertson, 2000).

In the work reported here, Raman spectra were excited in the near infrared with the defocused beam of a Nd:YAG laser ($\lambda = 1.064$ μm) to minimise thermal effects. Details of the technique were reported by Dippel, Jander, and Heintzenberg (1999). Raman spectra of soot samples from the AIDA chamber, collected on Nuclepore filters (pore diameter 0.2 μm) at the beginning and before the end of experiments 2, 3, 5, 6, and 7 (cf. Table 3), were recorded with a Bruker IFS 55 spectrometer fitted with a FRA-Raman module. The filters were masked to obtain two circular spots of 8 mm diameter. As exemplified by representative spectra of Diesel and "Palas" soot in

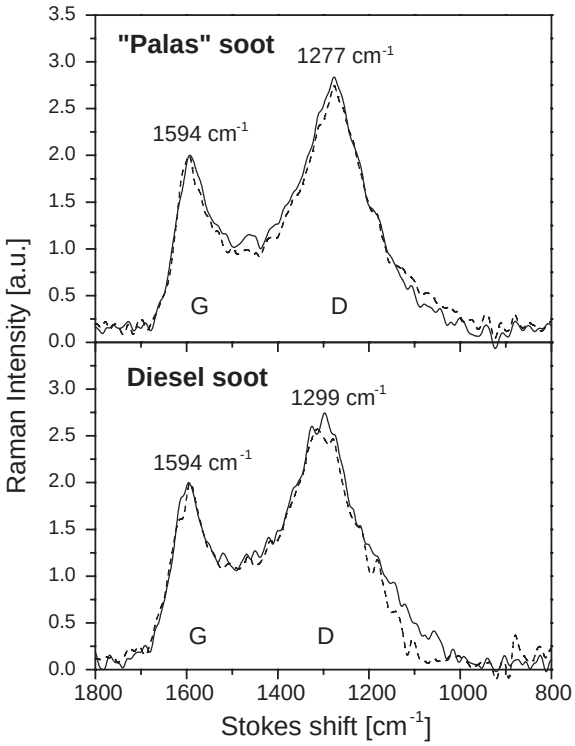

Fig. 3. Raman spectra of Diesel and "Palas" soot. The pairs of superimposed spectra refer to filter samples which were collected at the beginning (solid) and before the end (dashed lines) of experiments 2 (lower panel) and 3 (upper panel).

Fig. 3, the background-corrected spectra showed similar I_G/I_D ratios and bandwidths in all cases, irrespective of the soot type, sample age, absence/presence of ammonium sulphate particles on the filter, or absence/presence of organic coatings. This result is surprising in view of the significantly different nanostructures of Diesel and "Palas" soot as revealed by HRTEM, see the companion paper by Wentzel et al. (2003): according to the work of Tuinstra and Koenig (1970), these different nanostructures should give rise to significantly different I_G/I_D ratios, in clear contrast to our results. However, while the G bands were always coincident within error limits, a small but significant red shift of the D band, from 1299 cm^{-1} in Diesel soot to 1277 cm^{-1} in "Palas", was detected. This shift may be indicative of different degrees of disorder in these materials.

Another means of differentiation between different degrees of disorder in soot is electron spin resonance (ESR) spectroscopy. This technique was first applied to crystallographically oriented samples of graphite monocrystals by Wagoner (1960) who showed that the anisotropic signal is due to conduction electrons. Although the line shape became more symmetric when samples of very small randomly oriented graphitic microcrystallites were studied, it was shown theoretically that the ESR line should remain slightly asymmetric (Singer and Wagoner, 1962), in contrast to the perfectly symmetric resonances which have been measured with various "amorphous" carbon samples (Yordanov, Veleva, & Christov, 1996; Chughtai, Atteya, Kim, Konowalchuk, & Smith, 1998; Yordanov, 1999). These symmetric resonances have been attributed to radical sites rather than to conduction electrons (Kawamura, 1998).

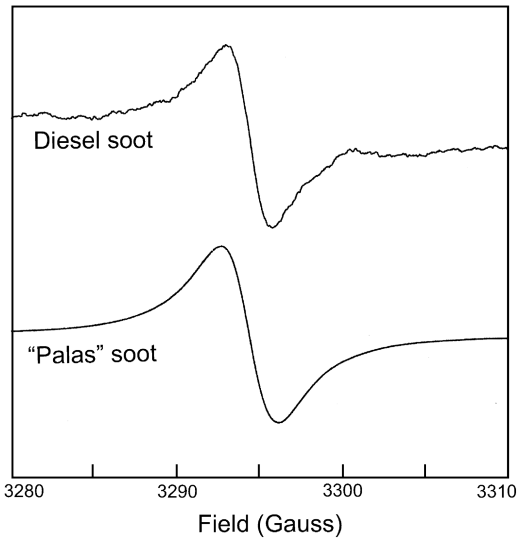

Fig. 4. ESR spectra of "Palas" and Diesel soot, suspended and frozen in benzene, $T = 77$ K.

The ESR spectra reported in this work were recorded on a Bruker ESP 300E spectrometer with an ER 4109 WZS widebore cavity. Highly dispersed soot samples were prepared by passing "Palas" or Diesel soot aerosol through ESR-silent quartz tubes of 2.54 mm i.d. which were loosely packed with 150 mg ultra pure quartz wool. The quartz tubes could be directly introduced into the ESR cavity of a 12 inch magnet (Varian). Spectra were recorded while the quartz tubes were purged with Ar (6.0, Messer Griesheim). Similar spectra, but with better signal-to-noise ratios, were obtained by ultrasonically dispersing soot samples in benzene. The dispersions were immediately frozen to prevent coagulation and settling of the particles. Representative spectra of "Palas" and Diesel soot dispersions, recorded at 77 K, are shown in Fig. 4. From a large number of ESR spectra obtained at room temperature by the quartz wool technique, the following g-factors and line widths were determined:

$$\text{"Palas"soot}: \; g = 2.0035 \pm 0.0004; \quad \Delta H_{pp} = 2.4 \pm 0.4 \text{ G}.$$

$$\text{Diesel soot}: \; g = 2.0039 \pm 0.0005; \quad \Delta H_{pp} = 2.5 \pm 0.4 \text{ G}.$$

Similar g-values but often considerably larger line widths are reported in the literature, e.g. for atmospheric soot samples collected on filters (Yordanov, 1999).

The g-values and line widths reported above do not reveal significant differences between "Palas" and Diesel soot. However, ESR spectra of Diesel soot were notoriously less intense than spectra of "Palas" soot. Therefore, spin densities were also determined. For this purpose, ESR spectra of various amounts of either Diesel or "Palas" soot deposited on quartz wool plugs were recorded. Subsequently the amounts of CO_2 resulting from the quantitative combustion of the deposits were determined by automated coulometric titration (Saathoff et al., 2003a). This yielded *relative* spin densities for both materials. Absolute data were obtained by calibrating the ESR spectrometer with quartz wool plugs which had been coated under oxygen-free conditions with a stable organic free radical compound

(DPPH = 1.1-Diphenyl-1-pikrylhydrazyl, $C_8H_{12}N_5O_6$). The amounts of DPPH deposited on the quartz wool plugs were determined in terms of their carbon contents by combustion, using automated coulometric detection of the evolved CO_2, as described above. In this way the following spin densities were determined:

"Palas" soot : $(7 \pm 2) \times 10^{-4}$ spins per C-atom.

Diesel soot : $(8 \pm 3) \times 10^{-5}$ spins per C-atom.

The result for Diesel soot falls within the range of reported spin densities of similar materials (Adriaanse, Brom, Michels, & Brokken-Zijp, 1997; Chughtai et al., 1998). The exceptionally large spin density of "Palas" soot is taken as evidence that this material is significantly less ordered than Diesel soot.

It is well known that the ESR signal of soot is attenuated by paramagnetic gases (Chughtai et al., 1998). In fact, up to 25% of the initial ESR signal of "Palas" soot could be quenched by adding up to 1 vol% NO_2 to the purge gas. The effect showed a tendency to level off well before 50% of the initial signal had been quenched. The effect was completely reversible, i.e. the original signal was restored when the samples were purged with pure N_2 or Ar for a few minutes. Quenching experiments with Diesel soot yielded qualitatively similar results.

We have evidence from combustion experiments (Kamm, 2000) that the ESR-active sites of "Palas" and Diesel soot are homogeneously distributed over the volume of the particles. Consider the following example: a spherical "Palas" soot particle with a typical diameter of 8 nm consists of roughly 27000 carbon atoms, which carry about 19 ESR-active electrons. About 7700 of the carbon atoms are exposed at the particle surface, assuming a surface density of 3.8×10^{15} C cm^{-2}, similar to a graphene sheet. Therefore, the average number of ESR-active surface sites is less than 6 per particle. Although the diameter of Diesel primaries is significantly larger ($\sim$30 nm), the number of ESR-active surface sites per particle is only about twice as large, owing to the much lower spin density.

We can only speculate about the nature of the ESR-active sites: soot particles are believed to consist of more or less disorderly stacked 6- and 5-membered PAH-like graphene sheets (Homann, 1998). Stable PAHs are dressed with an even number of hydrogen atoms at their periphery, while those ring systems which carry an odd number of hydrogen atoms are π-radicals with an unpaired electron. For example, the smallest unstable PAH with an odd number of hydrogen atoms, $C_{13}H_9$, consists of three annealed 6-membered rings which form a planar molecule of D_{3h} symmetry. The unpaired electron makes these PAHs unstable in the gas phase, and so far only their rather stable cations have been observed (Homann, 1998). However, large PAH-like graphene sheets with an odd number of electrons are likely to be stabilised by incorporation in a soot particle, thus giving rise to an ESR signal. If the spin density of such partially delocalised electrons is non-zero at the particle surface, their ESR signal is amenable to quenching by gaseous free radicals such as NO_2, in agreement with observation.

4. Outline of the campaign

We shall now briefly lead through the 10 experiments (Table 3), which were carried out during the soot characterisation campaign at the AIDA facility. The interested reader is encouraged to

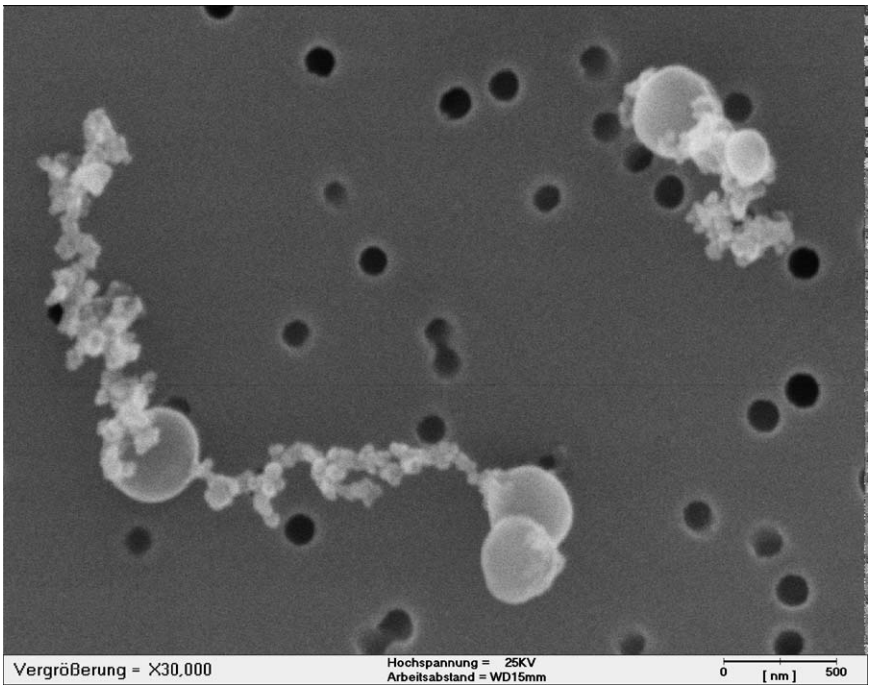

Fig. 5. SEM picture of particles collected 41 h after an external mixture of Diesel soot and ammonium sulphate aerosols had been introduced into the AIDA chamber: some mixed particles have been formed due to coagulation. The larger spheres are $(NH_4)_2SO_4$-particles which are attached to agglomerates of much smaller soot monomers.

consult the companion papers where specific results of the experiments are presented and discussed in depth. Common to all experiments was a careful characterisation of the mass and composition of the aerosols, particularly at the beginning and before the termination of each experiment (Saathoff et al., 2003a).

Experiment 1 with pure "Palas" soot served mainly as a performance test of the experimental equipment (cf. Tables 1 and 2) which had been assembled around the AIDA chamber, and for this purpose was done in pure dry synthetic air. Experiments 2 and 3 were carried out with humidified air in the presence of NO_x, to study various properties of "Palas" and Diesel soot aerosols under environmentally relevant conditions. The companion paper by Wentzel et al. (2003) should be consulted for a detailed intercomparison between the measured time evolution and the simulated dynamics of the fractal aerosols which were computed with the COSIMA code (Naumann, 2003). Wentzel et al. (2003) focus on the determination of the microstructure and fractal dimension of soot particles, (a) on the basis of fractal scaling laws, and (b) by directly evaluating a large number of transmission electron micrographs. The COSIMA code was also utilised to interpret the optical properties of soot aerosols, which were measured redundantly with several in situ and ex situ techniques. The results are presented in the companion papers by Schnaiter et al. (2003) and Weingartner et al. (2003).

The purpose of experiments 5 and 6 (including reference experiment 4 with pure ammonium sulphate aerosol) was to study the eventual transition from an external mixture of ammonium sulphate aerosol with Diesel soot to an internally mixed aerosol, focussing mainly on optical properties.

Fig. 5 shows a SEM picture of mixed particles which were sampled 41 h after an external mixture of Diesel soot and ammonium sulphate aerosol had been prepared in the AIDA chamber. TEM images of mixed particles can also be found in the companion paper by Wentzel et al. (2003). The papers by Schnaiter et al. (2003) and Weingartner et al. (2003) should be consulted for results of the optical measurements.

The subsequent series of experiments, 7–9, and a reference experiment 10 in the absence of seed aerosol, was devoted to the study of coating effects. "Palas" soot, Diesel soot, and ammonium sulphate aerosols were coated in situ with products of the α-pinene + ozone reaction, cf. Section 2.2 above. A detailed account of these experiments, including new particle formation by homogeneous nucleation in the absence of seed aerosol, experiment 10, is given in a companion paper by Saathoff et al. (2003b). Coatings with optically non-absorbing organic material affect the hygroscopic properties of the soot particles, their fractal structure, and in particular their optical properties (Schnaiter et al., 2003; Weingartner et al., 2003; Saathoff et al., 2003b). The coated aerosols were also used as test materials to study the performance of single particle mass spectrometry and other depth profiling techniques, cf. Section 3.3 above. Details are presented in the companion paper by Kirchner et al. (2003).

5. Summary

The technical infrastructure and the strategy of the AIDA Soot Characterisation Campaign 1999 have been outlined, with references to companion papers where specific results of the experiments can be found. Raman and ESR spectra of Diesel soot and "Palas" soot from a spark discharge generator are presented, and spin density measurements based on quantitative ESR spectroscopy are discussed with regards to microstructural differences between these materials. While the Raman and ESR spectra were nearly indistinguishable, except for a high frequency shift of the D-band in "Palas", an order of magnitude difference was found between the spin densities in both materials. It is proposed that π-radicals contribute to the ESR spectra of "Palas" and Diesel soot. PAH-like graphene sheets with an odd number of peripheral hydrogen atoms are π-radicals which would be unstable in the gas phase, but may be "frozen", and thus stabilised, by incorporation into soot particles. The π-radical electron may interact with the unpaired electron of adsorbed free radical species, in agreement with the reversible quenching effect of NO_2. The larger spin density of "Palas" soot is indicative of a higher degree of disorder or metastability in this material. It is shown that the number of ESR-active radical sites at the surface of soot is too low to affect the chemisorptive properties of soot aerosol to a significant extent.

Acknowledgements

We would like to acknowledge the valuable technical assistance of Elisabeth Kranz, Rainer Buschbacher, Peter Müsgen and Georg Scheurig. This work was partially supported by the German Ministry of Education and Research (BMBF), grant No 07AF209.

References

Adriaanse, L. J., Brom, H. B., Michels, M. A. J., & Brokken-Zijp, J. C. M. (1997). Electron localization in a percolating network: An ESR study of carbon-black/polymer composites. *Physical Review B*, *55*, 9383–9386.

Arens, F., Gutzwiller, L., Baltensperger, U., Gäggeler, H. W., & Ammann, M. (2001). Homogeneous reaction of NO_2 on diesel soot particles. *Environmental Science and Technology*, *35*, 2191–2199.

Baltensperger, U., Weingartner, E., Burtscher, H., & Keskinen, J. (2001). Dynamic mass and surface area measurements. In K. Willeke, & P. A. Baron (Eds.), *Aerosol measurement: Principles, techniques and applications* (2nd ed.). Chichester, New York: Wiley.

Berghmans, P., Pauwels, J., Roekens, E., & Bogaert, R. (1996). Comparison of methods for the concentration measurement of black (carbonaceous) aerosol in ambient air. *Journal of Aerosol Science*, *27*, 689–690.

Blake, D. F., & Kato, K. (1995). Latitudinal distribution of black carbon soot in the upper troposphere and lower stratosphere. *Journal of Geophysical Research*, *100*, 7195–7202.

Bunz, H., Möhler, O., Naumann, K.-H., Saathoff, H., Schöck, W., & Schurath, U. (1996). The novel aerosol chamber facility AIDA: Status and first results. *Proceedings of the EU symposium on the physico-chemical behaviour of atmospheric pollutants*, Venice, Italy.

Burtscher, H. (1992). Measurement and characteristics of combustion aerosols with special consideration of photoelectric charging and charging by flame ions. *Journal of Aerosol Science*, *23*, 549–595.

Burtscher, H., & Siegmann, H. C. (1994). Monitoring PAH-emissions from combustion processes by photoelectric charging. *Combustion Science and Technology*, *101*, 327–332.

Chughtai, A. R., Atteya, M. M. O., Kim, J., Konowalchuk, B. K., & Smith, D. M. (1998). Adsorption and adsorbate interaction at soot particle surfaces. *Carbon*, *36*, 1573–1589.

Cooke, W. F., Liousse, C., Cachier, H., & Feichter, J. (1999). Construction of a $1^\circ \times 1^\circ$ fossil fuel emission data set for carbonaceous aerosol and implementation and radiative impact in the ECHAM4 model. *Journal of Geophysical Research*, *104*, 22137–22162.

Cooke, W. F., & Wilson, J. J. N. (1996). A global black carbon aerosol model. *Journal of Geophysical Research*, *101*, 19395–19409.

Dillmann, H.-G., Bier, W., Linder, G., & Schubert, K. (1987). Measurement of removal efficiencies performed on powder metal and fibre metal cartridges to be used in Uranium enrichment facilities and glovebox exhaust ducts. In: M. W. First (Ed.), *Proceedings of the 19th DOE/NRC nuclear air cleaning conference*, Seattle, August 1986.

Dippel, B., Jander, H., & Heintzenberg, J. (1999). NIR FT Raman spectroscopic study of flame soot. *Physical Chemistry and Chemical Physics*, *1*, 4707–4712.

Disselkamp, R. S., Carpenter, M. A., & Cowin, J. P. (2000a). A chamber investigation of nitric acid—soot aerosol chemistry at 298 K. *Journal of Atmospheric Chemistry*, *37*, 113–123.

Disselkamp, R. S., Carpenter, M. A., Cowlin, J. P., Berkowitz, C. M., Chapman, E. G., Zaverin, R. A., & Laulainen, N. S. (2000b). Ozone loss in soot aerosol. *Journal of Geophysical Research*, *105*, 9767–9771.

Dockery, D. W., Pope III, C. A., Xu, X., Spengler, J. D., Ware, J. H., Fay, M. E., Ferris, B. G., & Speizer, F. E. (1993). An association between air pollution and mortality in six U.S. cities. *The New England Journal of Medicine*, *329* (24), 1753.

Dod, R. L., Giauque, R. D., Novakov, T., Su, W., Zhang, Q., & Song, W. (1986). Sulfate and carbonaceous aerosols in Beijing, China. *Atmospheric Environment*, *11*, 2271–2275.

Ferrari, A. C., & Robertson, J. (2000). Interpretation of Raman spectra of disordered and amorphous carbon. *Physical Review B*, *61*, 14095–14107.

Grassian, V. H. (2001). Heterogeneous uptake and reaction of nitrogen oxides and volatile organic compounds on the surface of atmospheric particles including oxides, carbonates, soot and mineral dust: Implications for the chemical balance of the troposphere. *International Review of Physical Chemistry*, *20*, 467–548.

Griffin, R. J., Cocker III, D. R., Flagan, R. C., & Seinfeld, J. H. (1999). Organic aerosol formation from the oxidation of biogenic hydrocarbons. *Journal of Geophysical Research*, *104*, 3555–3567.

Gysel, M., Weingartner, E., & Baltensperger, U. (2002). Hygroscopicity of aerosol particles at low temperatures. 2. Theoretical and experimental hygroscopic properties of laboratory generated aerosols. *Environmental Science and Technology*, *36*, 63–68.

Hansen, A. D. A., & Novakov, T. (1990). Real-time measurement of aerosol black carbon during the carbonaceous species methods comparison study. *Aerosol Science and Technology*, *12*, 194–199.

Heintzenberg, J., & Winkler, P. (1991). Elemental carbon in the atmosphere: Challenges for the trace analyst. *Fresenius Journal of Analytical Chemistry*, *340*, 540–543.

Helsper, C., Mölter, W., Löffler, F., Wadenpohl, C., Kaufmann, S., & Wenninger, G. (1993). Investigation of a new aerosol generator for the production of carbon aggregate particles. *Atmospheric Environment*, *27A*, 1271–1275.

Hitzenberger, R., & Tohno, S. (2001). Comparison of black carbon (BC) aerosols in two urban areas—concentrations and size distributions. *Atmospheric Environment*, *35*, 2153–2167.

Homann, K.-H. (1998). Fulleren- und Rußbildung—Wege zu großen Teilchen in Flammen. *Angewandtl Chemie*, *110*, 2572–2590.

Horvath, H. (1997). Experimental calibration of aerosol light absorption measurements using the integrating plate method—Summary of the data. *Journal of Aerosol Science*, *28*, 1149–1161.

Intergovernmental Panel on Climate Change (IPCC) (2001). In J. T. Houghton, Y. Ding, D. J. Griggs, M. Noguer, P. J. van der Linden, & D. Xiaosu (Eds.), *Contribution of working group I to the third assessment report*: *Climate change 2001*: *The scientific basis*. Cambridge: Cambridge University Press.

Israel, G. W., Schlums, C., Treffeisen, R., & Pesch, M. (1996). *Rußimmission in Berlin*. Final report B 281 KF, VDI Verlag GmbH, Düsseldorf.

Jacob, D. J. (2000). Heterogeneous chemistry and tropospheric ozone. *Atmospheric Environment*, *34*, 2131–2159.

Kaiser, J. (2000). Evidence mounts that tiny particles can kill. *Science*, *289*(5476), 22–23.

Kamm, S., Möhler, O., Naumann, K.-H., Saathoff, H., & Schurath, U. (1999). The heterogeneous reaction of ozone with soot aerosol. *Atmospheric Environment*, *33*, 4651.

Kamm, S. (2000). Kinetische Untersuchungen der Oxidation von luftgetragenen Rußpartikeln mittels ESR- und FTIR-Spektroskopie. PhD-thesis, University of Heidelberg.

Kawamura, K. (1998). Electron spin resonance behavior of pitch-based carbons in the heat treatment temperature range of 1100–2000°C. *Carbon*, *36*, 1227–1230.

Kirchner, U., Scheer, V., & Vogt, R. (2000). FTIR spectroscopic investigation of the mechanism and kinetics of the heterogeneous reactions of NO_2 and HNO_3 with soot. *Journal of Physical Chemistry A*, *104*, 8908–8915.

Kirchner, U., Vogt, R., Natzeck, C., & Goschnick, J. (2003). Single particle MS, SNMS, SIMS, XPS, and FTIR spectroscopic analysis of soot particles during the AIDA campaign. *Journal of Aerosol Science*, *34*, 1323–1346.

Kittelson, D. B. (1998). Engines and nanoparticles: A review. *Journal of Aerosol Science*, *29*, 575–588.

Koch, D. (2001). Transport and direct radiative forcing of carbonaceous and sulfate aerosols in the GISS GCM. *Journal of Geophysical Research*, *106*, 20311–20332.

Koch, St., Winterhalter, R., Uherek, E., Kolloff, A., Neeb, P., & Moortgat, G. K. (2000). Formation of new particles in the gas-phase ozonolysis of monoterpenes. *Atmospheric Environment*, *34*, 4031–4042.

Krämer, L., Bozoki, Z., & Niessner, R. (2001). Characterisation of a mobile photoacustic sensor for atmospheric black carbon monitoring. *Analytical Science*, *17*, S563–S566.

Kuhlbusch, T. A. J., Andreae, M. O., Cachier, H., Goldammer, J. G., Lacaux, J.-P., Shea, R., & Crutzen, P. J. (1996). Black carbon formation by savannah fires: Measurements and implications for the global carbon cycle. *Journal of Geophysical Research*, *101*, 23651–23665.

Kuznetsov, B. V., Rakhmanova T. A., Popovitcheva O. B., & Shonia, N. K. (2003). Water adsorption and energetic properties of spark discharge soot: Specific features of hydrophilicity. *Journal of Aerosol Science*, in press.

Lavanchy, V. M. H., Gäggeler, H. W., Nyeki, S., & Baltensperger, U. (1999). Elemental carbon (EC) and black carbon (BC) measurements with a thermal method and an aethalometer at the high-alpine research station Jungfraujoch. *Atmospheric Environment*, *33*, 2759–2769.

Lelieveld, J., Crutzen, P. J., Ramanathan, V., Andreae, M. O., Brenninkmeijer, C. A. M., Campos, T., Cass, G. R., Dickerson, R. R., Fischer, H., de Gouw, J. A., Hansel, A., Jefferson, A., Kley, D., de Laat, A. T. J., Lal, S., Lawrence, M. G., Lobert, J. M., Mayol-Bracero, O. L., Mitra, A. P., Novakov, T., Oltmans, S. J., Prather, K. A., Reiner, T., Rodhe, H., Scheeren, H. A., Kikka, D., & Williams, J. (2001). The Indian ocean experiment: Widespread air pollution from south and southeast asia. *Science*, *291*, 1031–1036.

Liousse, C., Penner, J. E., Chuang, C., Walton, J. J., Eddleman, H., & Cachier, H. (1996). A global three-dimensional model study of carbonaceous aerosols. *Journal of Geophysical Research*, *101*, 19411–19432.

Matter, U., Siegmann, H. C., & Burtscher, H. (1999). Dynamic field measurement of submicron particles from diesel engines. *Environmental Science and Technology*, *33*, 1946–1952.

Morawska, L. (2001). New directions: Particle air pollution down under. *Atmospheric Environment*, *35*, 1711–1712.

Naumann, K.-H. (2003). COSIMA—a computer program simulating the dynamics of fractal aerosol. *Journal of Aerosol Science*, *34*, 1371–1397.

Naumann, K.-H., & Bunz, H. (1992). Computer simulations on the dynamics of fractal aerosols. *Journal of Aerosol Science*, *23*, 361–364.

Pakkanen, T. A., Kerminen, V. M., Ojanen, Ch. H., Hillamo, R. E., Aarnio, P., & Koskentalo, T. (2000). Atmospheric black carbon in Helsinki. *Atmospheric Environment*, *34*, 1497–1506.

Peters, A., Wichmann, H. E., Tuch, Th., Heinrich, J., & Heyder, J. (1997). Respiratory effects are associated with the number of ultrafine particles. *American Journal of Respiratory and Critical Care Medicine*, *155*, 1376–1383.

Pope III, C. A., Thun, M. J., Namboodiri, M. M., Dockery, D. W., Evans, J. S., Speizer, F. E., & Heath Jr., C. W. (1995). Particulate air pollution as a predictor of mortality in a prospective study of U.S. adults. *American Journal of Respiratory and Critical Care Medicine*, *151*, 669–674.

Pueschel, R. F., Boering, K. A., Verma, S., Howard, S. D., Ferry, G. V., Goodman, J., Allen, D. A., & Hamill, P. (1997). Soot aerosol in the lower stratosphere: Pole-to-pole variability and contributions by aircraft. *Journal of Geophysical Research*, *102*, 13113–13118.

Rajeev, K., & Ramanathan, V. (2001). Direct observations of clear-sky aerosol radiative forcing from space during the Indian ocean experiment. *Journal of Geophysical Research*, *106*, 17221–17235.

Ravishankara, A. R., & Longfellow, C. A. (1999). Reactions on tropospheric condensed matter. *Physical Chemistry and Chemical Physics*, *1*, 5433–5441.

Saathoff, H., Naumann, K.-H., Riemer, N., Kamm, S., Möhler, O., Schurath, U., Vogel, H., & Vogel, B. (2001). The loss of $NO_2, HNO_3, NO_3/N_2O_5$, and $HO_2/HOONO_2$ on soot aerosol: A chamber and modelling study. *Geophyical Research Letters*, *28*, 1957–1960.

Saathoff, H., Naumann, K.-H., Schnaiter, M., Schöck, W., Weingartner, E., Baltensperger, U., Krämer, L., Bozooi, Z., Pöschl, U., Niessner, R., & Schurath, U. (2003a). Carbon mass determination during the AIDA soot aerosol campaign 1999. *Journal of Aerosol Science*, *34*, 1399–1420.

Saathoff, H., Naumann, K.-H., Schnaiter, M., Schöck, W., Möhler, O., Schurath, U., Weingartner, E., & Baltensperger, U. (2003b). Coating of soot and $(NH_4)_2SO_4$ particles by ozonolysis products of α-pinene. *Journal of Aerosol Science*, *34*, 1297–1321.

Schnaiter, M., Horvath, H., Möhler, O., Naumann, K.-H., Saathoff, H., & Schöck, O. W. (2003). UV-VIS-NIR spectral optical properties of soot containing aerosols. *Journal of Aerosol Science*, *34*, 1421–1444.

Schwartz, J. (1993). Particulate air pollution and chronic respiratory disease. *Environmental Research*, *62*, 7.

Schwyn, S., Garwin, E., & Schmidt-Ott, A. (1988). Technical Note: Aerosol generation by spark discharge. *Journal of Aerosol Science*, *19*, 639–642.

Singer, L. S., & Wagoner, G. (1962). Electron spin resonance in polycrystalline graphite. *Journal of Chemical Physics*, *37*, 1812–1817.

Stöber, W., & Abel, U. R. (1996). Lung cancer due to diesel soot particles in ambient air? A critical appraisal of epidemiological studies addressing this question. *International Archives of Occupational and Environmental Health*, *68* (Suppl), S3–S61.

Strawa, A. W., Drdla, K., Ferry, G. V., Verma, S., Pueschel, R. F., Yasuda, M., Salawitch, R. J., Gao, R. S., Howard, S. D., Bui, P. T., Loewenstein, M., Elkins, J. W., Perkins, K. K., & Cohen, R. (1999). Carbonaceous aerosol (soot) measured in the lower stratosphere during POLARIS and its role in stratospheric photochemistry. *Journal of Geophysical Research*, *104*, 26753–26766.

Streets, D. G., Gupta, S., Waldhoff, S. T., Wang, M. Q., Bond, T. C., & Yiyun, Bo. (2001). Black carbon emissions in China. *Atmospheric Environment*, *35*, 4281–4296.

Sze, S.-K., Siddique, N., Sloan, J. J., & Escribano, R. (2001). Raman spectroscopic characterization of carbonaceous aerosols. *Atmospheric Environment*, *35*, 561–568.

Trimborn, A., Hinz, K.-P., & Spengler, B. (2000). Online analysis of atmospheric particles with a transportable laser mass spectrometer. *Aerosol Science and Technology*, *33*, 191–201.

Tuinstra, F., & Koenig, J. L. (1970). Raman spectrum of graphite. *Journal of Chemical Physics*, *53*, 1126–1130.

Wagoner, G. (1960). Spin resonance of charge carriers in graphite. *Physical Review*, *118*, 647–663.

Wakayama, H., Mizuno, J., Fukushima, Y., Nagano, K., Fukunaga, T., & Mizutani, U. (1999). Structural defects in mechanically ground graphite. *Carbon*, *37*, 947–952.

Weingartner, E., Gysel, M., & Baltensperger, U. (2002). Hygroscopicity of aerosol particles at low temperatures. 1. New low-temperature H-TDMA instrument: Setup and first applications. *Environmental Science and Technology*, *36*, 55–62.

Weingartner, E., Saathoff, H., Schnaiter, M., Streit, N., Bitnar, B., & Baltensperger, U. (2003). Absorption of light by soot particles: Determination of the absorption by means of aethalometers. *Journal of Aerosol Science*, *34*, 1445–1463.

Weingartner, E., Streit, N., Baltensperger, U., Saathoff, H., Schnaiter, M., Schurath, U., Kirchner, U., & Lavanchy, V. (2000). *Characterization of fresh and aged soot particles*, PSI scientific report 1999, Vol. 1 (p. 157).

Wentzel, M., Gorzawski, H., Naumann, K.-H., Saathoff, H., & Weinbruch, S. (2003). Transmission electron microscopical and aerosol dynamical characterisation of soot aerosols. *Journal of Aerosol Science, 34*, 1347–1370.

Wichmann, H.-E., & Peters, A. (2000). Epidemiological evidence of the effects of ultrafine particle exposure. *Philosophical Transactions of the Royal Society of London A*, *358*, 2751–2769.

Yordanov, N. D. (1999). Introduction to the theory of electron paramagnetic resonance and its application to the study of aerosols (pp. 197–213). In K. R. Spurny (Ed.), *Analytical chemistry of aerosols*, Boca Raton: Lewis Publishers.

Yordanov, N. D., Veleva, B., & Christov, R (1996). EPR study of aerosols with carbonaceous products in the urban air. *Applied Magnetic Resonace*, *10*, 439–445.

Yu, J., Cocker III, D. R., Griffin, R. J., Flagan, R. C., & Seinfeld, J. H. (1999). Gas-phase ozone oxidation of monoterpenes: Gaseous and particulate products. *Journal of Atmospheric Chemistry*, *34*, 207–258.